Available online at www.sciencedirect.com
SCIENCE DIRECT®
Journal of Power Sources 136 (2004) 99–107
JOURNAL OF POWER SOURCES
www.elsevier.com/locate/jpowsour

Development of a simulator for both property and safety of a lithium secondary battery

Takashi Yamauchi [a,*], Koichi Mizushima [b], Yuji Satoh [a], Shuji Yamada [c]

[a] *Power Supply Materials and Devices Laboratory, Corporate Research and Development Center, Toshiba Corporation, Kawasaki, Kanagawa 212-8582, Japan*
[b] *Toshiba Research Consulting Company, Toshiba Corporation, Kawasaki, Kanagawa 212-8582, Japan*
[c] *Advanced Discrete Semiconductor Technology Laboratory, Corporate Research and Development Center, Toshiba Corporation, Kawasaki, Kanagawa 212-8582, Japan*

Received 13 February 2004; received in revised form 8 April 2004; accepted 10 May 2004

Abstract

We propose a model of lithium secondary batteries for analyzing both charging/ discharging characteristics and the increase of cell temperature in the case of the internal short circuit. We give an explanation to the experimental results of the nail penetration tests and discuss the structure-dependent properties of the batteries from the viewpoint of balance between energy density and safety. In particular, it is suggested that the thermal runaway in the nail penetration tests is determined by the total amount of Joule heat produced by the large current due to the internal short circuit until the discharge of the whole electrode is completed.

Keywords: Lithium battery; Simulation; Safety; Short circuit; Thermal runaway

1. Introduction

For lithium secondary batteries, high energy density, good high-rate performance, long cycle life and safety are required for the application to portable equipments. This paper focuses on the improvement of both high-rate performance and safety for a lithium battery by optimizing its constructional factors. In particular, in regard to safety, we discuss the increase of cell temperature in the case of the internal short circuit, which is considered to have an important bearing on the discharge characteristics of the battery, as mentioned in the following. For example, it can be easily understood that high energy density leads to the large increase of cell temperature in the event of an internal short circuit. In addition, the nail penetration test results for two batteries, whose rate dependences of capaciy are shown in Fig. 1, have been reported to show that the battery with a better high-rate performance has a higher possibility for the thermal runaway to take place at the short circuit, in whose electrodes the diffusion of lithium ions is designed to become faster [1]. Although these phenomena need to be taken into consideration in the battery design, satisfactory explanations have not been given to them theoretically. Thus, in this paper, we proposed a model of lithium secondary batteries for analyzing both charging/discharging characteristics and the increase of cell temperature in the case of the internal short circuit, in order to obtain physical insights into these phenomena.

Lithium batteries have been the subject of a number of studies employing thermal simulation [2–5], although the proposed models have not been adapted to the issue of the thermal runaway in the nail penetration tests. However, in the case of a short circuit, the heat transfer in the cell or to the surroundings, which have been treated strictly in these studies, can be neglected, since the rapid increase of cell temperature and the thermal runaway takes place within a few seconds after a nail is inserted in the battery. That is, only if we calculate the total amount of the Joule heat produced by the large current due to the internal short circuit and compare the cell temperature obtained by dividing it by the heat capacity of the cell with the critical temperature for thermal runaway, we can explain the nail penetration test results for batteries with different high-rate performances or discharge capacities. We can consider that the large current is produced locally around the regions of the electrode sheet wound in

* Corresponding author. Tel.: +81 44 549 2126; fax: +81 44 520 1286.
E-mail address: ytakashi.yamauchi@toshiba.co.jp (T. Yamauchi).

0378-7753/$ – see front matter © 2004 Elsevier B.V. All rights reserved.
doi:10.1016/j.jpowsour.2004.05.011

Nomenclature

C	lithium concentration in the electrode (mol/cm^3)
$\tilde{d}$	distance between the short-circuit regions (cm)
$\tilde{D}$	effective chemical diffusion constant of the electrode (cm^2/s)
E	electric field produced in the cathode (V/cm)
F	Faraday's constant (C/mol)
h	width of the electrode sheet (=5.425 cm)
H	specific heat of the electrode sheet (W/(cm^3 K))
I	discharge current per unit area of the tab (A/cm^2)
J	current density (A/cm^2)
L	length of the current collector (cm)
n	turn number of the electrode sheet
N	flux density (mol/(cm^2 s))
q	chemical reaction heat generated in the unit area of the electrode sheet (J/cm^2)
R	gas constant (J/(mol K))
R_c	$= \rho_c\gamma_c/hL$ (Ω)
t	time (s)
$\tilde{t}$	time taken for a nail to penetrate the battery (ms)
t_{LCD}	time taken for the large current discharge, due to the short circuit, to end (s)
T	cell temperature (K)
T_0	room temperature (=293 K)
T_m	maximum value of T in the direction z (K)
V	voltage (V)
$\tilde{V}$	molar volume (cm^3/mol)
V_p	potential difference between the electrodes (V)
$V_{p,rev}$	potential difference between the electrodes when the cell operates reversibly (V)
W	heat amount generated for a unit time in the unit volume of the electrode sheet (J/(s cm^3))
x	lithium composition

Greek letters

γ	thickness (μm)
γ_t	total thickness of the cathode/separator/anode assembly ($=\gamma_a+\gamma_s+\gamma_c$) ($\mu$m)
η_c	overvoltage ascribed to the contact resistance between the Li_xNiO_2 particles (V)
ρ_c	resistivity due to the contact between the Li_xNiO_2 particles (Ω cm)
σ	conductivity (S/cm)

Subscripts

a	anode
ac	current collector of the anode
c	cathode
cc	current collector of the cathode
e	electron
l	lithium ion
s	separator

the cell, which the nail passes through, and held until the cathode surface saturation with lithium occurs. The current distribution on the electrode sheet in the case of the internal short circuit can be calculated by using the same model as that for the usual discharge mode. Basically, this simulation was carried out by solving the equations self-consistently, which take into account both the electron transport in the current collectors and the lithium ion transport in the positive electrode/ separator/ negative electrode assembly. Moreover, we adopted the model of porous insertion electrodes with electrolyte, which was proposed for the Li/TiS_2 battery system [6–9]. However, in this work, we studied the properties of the lithium ion cell using Li_xNiO_2 as its active cathode material, whose safety has been improved with a view to its practical use. Thus, we took into account the overvoltage ascribed to the contact resistance between the Li_xNiO_2 cathode particles in our model, since it is considered to be not negligible due to the oxide layer on their surface [1,10]. It was found from the calculation results that the model proposed in this paper aids us in the design of lithium battery systems, although it is too crude for a quantitative analysis.

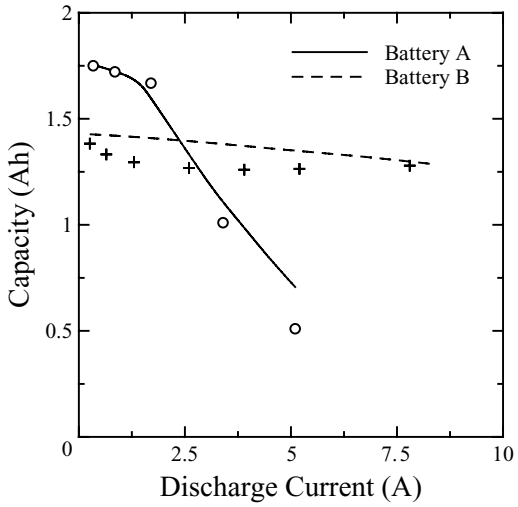

Fig. 1. Rate dependences of the capacity for batteries A and B. Both blank circles and crosses stand for the experimental data [1]. Both solid and dashed lines are the simulation results.

2. Formulation

2.1. Model for charging/discharging characteristics

The electrode sheet is spirally wound in the cylindrical (18650) type of lithium secondary battery, which consists of the thin sheets of the positive and negative electrodes, the separators and the current collectors of both electrodes as shown in Fig. 2. In this paper, the active cathode material is Li_xNiO_2, the active anode material is Li_xC_6, and the electrolyte system is 1 M solution of $LiPF_6$ in ethylene carbonate-ethyl methyl carbonate (EC-EMC). The directions of the current densities J_{ac}, J_s and J_{cc} in the discharge mode are illustrated in Fig. 2. Here, we regarded the current density distribution as uniform in the direction perpendicular to the cross-section of the electrode sheet shown in Fig. 2, since the width of the electrode sheet h is at most 5.425 cm. Namely, if we take the vertical direction as y and the horizontal direction as z, the equations of current conservation can be represented as follows:

$$\gamma_{cc}\frac{\partial J_{cc}}{\partial z} = -2J_s(z,t) + I_{cc}(z)$$
$$\gamma_{ac}\frac{\partial J_{ac}}{\partial z} = 2J_s(z,t) + I_{ac}(z) \quad (1)$$

where $\gamma_{ac,cc}$ are the thicknesses of the current collectors of the anode and the cathode, respectively. The current densities $I_{ac}(z)$ and $I_{cc}(z)$ at the ends of current collectors are obtained by dividing the discharge current by the area of the tab and defined as positive/negative in the discharge/charge mode, respectively. Moreover, since the migration of lithium ions contributes to the current density J_s in the separator dominantly, the relation between the current densities J_{ac}, J_s, J_{cc} and the voltages in the current collectors $V_{ac}(z,t)$, $V_{cc}(z,t)$ can be given by

$$J_{cc}(z,t) = -\sigma_{cc}\frac{\partial V_{cc}}{\partial z}$$
$$J_{ac}(z,t) = -\sigma_{ac}\frac{\partial V_{ac}}{\partial z} \quad (2)$$
$$V_{cc}(z,t) - V_{ac}(z,t) = J_s(z,t)\frac{\gamma_s}{\sigma_s} + V_p(z,t)$$

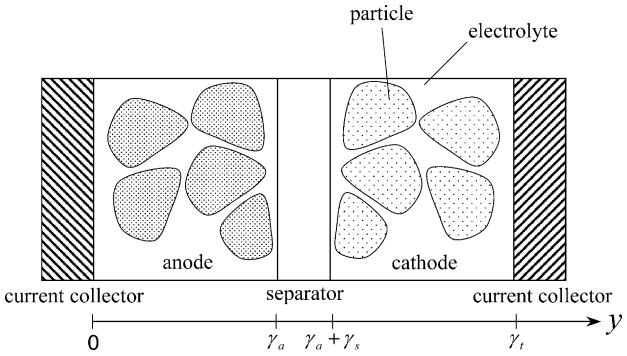

Fig. 3. Schematic diagram of the current collector/insertion anode/separator/insertion cathode/current collector cell.

where γ_s and σ_s denote the thickness of the separator and the electrolytic conductivity in the separator, which can be estimated as $4\exp(1250(1/298-1/T))$ mS/cm if the porosity of the separator is 0.5 [11,12]. $\sigma_{ac,cc}$ stands for the conductivities of current collectors of the negative and positive electrodes, respectively. As defined later, V_p denotes the potential difference between the electrodes.

Many models of porous insertion electrodes with organic electrolyte were proposed for the Li/TiS_2 battery system [6–9]. As shown in Fig. 3, both the diffusion in the active material particles and the migration in the electrolyte between the particles are taken into account in these models. The studies based on these models concluded that the capacity obtainable at a given discharge current is limited by the cathode surface saturation with lithium, if the electrolyte depletion does not occur in the porous electrode [6,9]. In this paper, we represented the lithium ion transport in the porous electrodes by a diffusion equation with an effective chemical diffusion constant $\tilde{D}$. Moreover, since the contact resistance between the Li_xNiO_2 cathode particles is not negligible due to the oxide layer on their surface, we took into account the drift of an electron in our transport model. That is, noting that $\sigma_l \ll \sigma_e$ and that the diffusion term is negligibly small comparing with the drift term in regard to an electron transport in the cathode, we reduced the Nernst–Planck equation

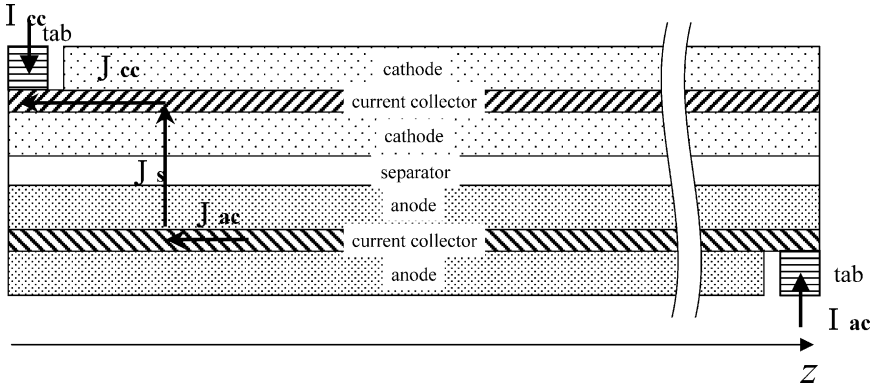

Fig. 2. Schematic diagram of the electrode sheet consisting of the positive and negative electrodes, the separators and the current collectors of both electrodes. The directions of the current densities J_{ac}, J_s and J_{cc} in the discharge mode are shown on this figure.

[9,13] as follows:

$$N_{\mathrm{l}} = -\tilde{D}_{\mathrm{c}}\frac{\partial C_{\mathrm{c}}}{\partial y}$$
$$N_{\mathrm{e}} = -\frac{\sigma_{\mathrm{e}}}{F}E \tag{3}$$

where $N_{\mathrm{l,e}}$, C_{c} and E stand for the flux density of a lithium ion, that of an electron, the lithium ion concentration and the electric field in the cathode, respectively. σ_{e} denotes the conductivity for an electron in the cathode. Here, we assumed that the effective chemical diffusion constant $\tilde{D}$ is treated as independent of the lithium ion concentration, for the following two reasons. Namely, we have only very sparse information available on this dependence and can consider that the most of calculation results shown in this paper are not modified by the concentration dependence. Therefore, the transport equation for a lithium ion in the cathode can be written similarly to that in the anode as follows:

$$\frac{\partial C_{\mathrm{a,c}}}{\partial t}(y,z,t) = \tilde{D}_{\mathrm{a,c}}\frac{\partial^2 C_{\mathrm{a,c}}}{\partial y^2}(y,z,t). \tag{4}$$

where C_{a} denotes the lithium ion concentration in the anode. We used the following boundary conditions for solving the Eq. (4).

$$\tilde{D}_{\mathrm{c}}\frac{\partial C_{\mathrm{c}}}{\partial y}(\gamma_{\mathrm{a}}+\gamma_{\mathrm{s}},z,t) = -\frac{J_{\mathrm{s}}(z,t)}{F}$$
$$\tilde{D}_{\mathrm{c}}\frac{\partial C_{\mathrm{c}}}{\partial y}(\gamma_{\mathrm{t}},z,t) = 0$$
$$\tilde{D}_{\mathrm{a}}\frac{\partial C_{\mathrm{a}}}{\partial y}(\gamma_{\mathrm{a}},z,t) = -\frac{J_{\mathrm{s}}(z,t)}{F} \tag{5}$$
$$\tilde{D}_{\mathrm{a}}\frac{\partial C_{\mathrm{a}}}{\partial y}(0,z,t) = 0$$

Moreover, we defined the potential difference between the electrodes V_p as follows:

$$V_p(z,t) = \mu_{\mathrm{c}}(\tilde{V}_{\mathrm{c}}C_{\mathrm{c}}(\gamma_{\mathrm{a}}+\gamma_{\mathrm{s}},z,t)) - \mu_{\mathrm{a}}(\tilde{V}_{\mathrm{a}}C_{\mathrm{a}}(\gamma_{\mathrm{a}},z,t)) - \eta_{\mathrm{c}}(z,t) \tag{6}$$

$$\eta_{\mathrm{c}}(z,t) \simeq \rho_{\mathrm{c}}\gamma_{\mathrm{c}}J_{\mathrm{s}}(z,t) \tag{7}$$

where $\mu_{\mathrm{a,c}}$ and $\tilde{V}_{\mathrm{a,c}}$ denote the open circuit voltages and the molar volumes of active material in the anode and the cathode, respectively. Eq. (6) means that the following two overvoltages cause the drop of cell voltage, namely, both the rate dependent overvoltage, which results from the concentration gradient of a lithium ion between the surface and the interior of the electrodes, and the overvoltage η_{c}, which is ascribed to the contact resistance between the $\mathrm{Li}_x\mathrm{NiO}_2$ cathode particles. In this paper, we represented η_{c} as $\rho_{\mathrm{c}}\gamma_{\mathrm{c}}J_{\mathrm{s}}$ and substituted the value obtained by the ac impedance measurement [1] into ρ_{c}. Moreover, referring to the papers [14,15], we analytically represented the open circuit voltages $\mu_{\mathrm{a,c}}$ as a function of lithium composition x by

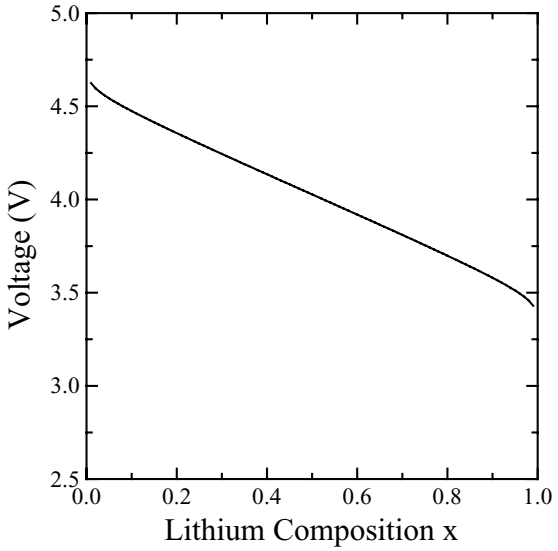

Fig. 4. Relation between the open circuit voltage in the cathode and lithium composition x.

$$\mu_{\mathrm{c}}(x) = A_1 + A_2x + \frac{RT}{F}\ln\left(\frac{x}{1-x}\right) \tag{8}$$

$$\mu_{\mathrm{a}}(x) = \sum_{i=1}^{5} B_i x^{-2(4-i)} + \frac{RT}{F}\ln\left(\frac{x}{1-x}\right) \tag{9}$$

where $A_i(1 \le i \le 2)$ and $B_i(1 \le i \le 5)$ are fitting parameters and were taken as 4.5, -9.7×10^{-1}, 7.4×10^{-11}, -1.9×10^{-8}, 5.1×10^{-4}, 9.2×10^{-2} and -1.7×10^{-2} [14,15], respectively. The results are shown in Figs. 4 and 5, respectively.

The above Eqs. (1)–(9) enable us to calculate the charging/discharging characteristics of the lithium ion battery. In

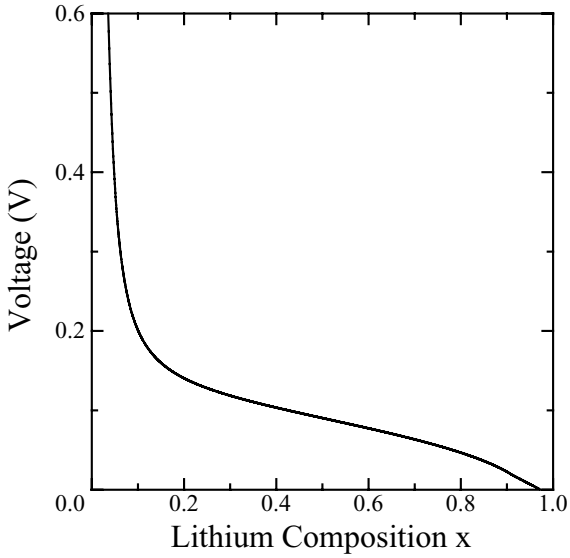

Fig. 5. Relation between the open circuit voltage in the anode and lithium composition x.

Table 1
Constructional parameters of batteries A and B used in the simulation

Constructional parameters	Battery A	Battery B
γ_{ac} (μm)	20	20
γ_a (μm)	95	44
γ_s (μm)	25	25
γ_c (μm)	75	33
γ_{cc} (μm)	20	20
L (cm)	43.5	80
R_c (m Ω)	90	47
$\tilde{V}_c$ (cm^3/mol)	35.5	35.5
$\tilde{V}_a$ (cm^3/mol)	9	9

this paper, we focus on the following two batteries which differ in both discharge capacity and high-rate performance. The values of the constructional parameters used in the simulation for these batteries are listed in the Table 1. Moreover, we took the effective chemical diffusion constants $\tilde{D}_c$ and $\tilde{D}_a$ as 1.8×10^{-8} cm^2/s and 1.0×10^{-7} cm^2/s, respectively, and assumed in the short-circuit simulation that they have the same dependence on the temperature as the conductivity of the electrolyte included in the electrodes. We show the calculation results of the discharge characteristics at room temperature for battery A in Fig. 6. It was found that the capacity is 1.75 Ah at 0.35 A (0.2C) and decreases rapidly with the increase in the discharge current. The rate dependence of capacity is illustrated as a solid line in Fig. 1. On the other hand, the broken line in Fig. 1 shows that the change in the capacity of battery B is less than 10% in the range of the discharge current between 0.28 A (0.2C) and 8.4 A (6C). Namely, battery B has a much better high-rate performance than battery A, although its capacity is lower. These rate dependences of capacity for these batteries obtained in this simulation can be found to show a qualitative agreement with those measured in the experiment [1]. In this paper, by analyzing the increase of cell temperature in the case of the internal short circuit for these batteries, we give an explanation to the experimental results of the nail penetration tests and clarify the principle factors that determine the thermal runaway in the nail penetration tests.

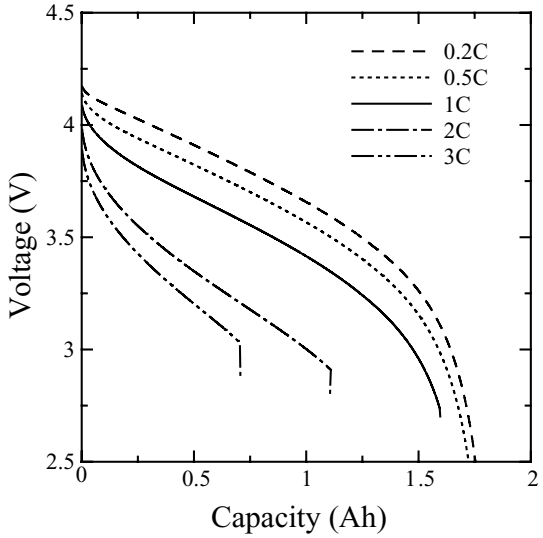

Fig. 6. Discharge characteristics for battery A in the current range from 0.2C (0.34 A) to 3C (5.1 A).

2.2. Short-circuit model

When a nail penetrates a lithium battery, the internal short circuit occurs at 2n regions of the electrode sheet wound n times in the cell, which are represented by the shaded areas in Fig. 7 and, hereafter, we call these regions the short-circuit regions. Namely, the width of this region can be regarded as nearly equal to the diameter of the nail (=1.5 mm). Moreover, as shown in Fig. 7, we can consider that the large current due to the short circuit is produced locally around these regions respectively and the discharge process continues in the electrode sheet until the cathode/separator interface becomes saturated with lithium. The sheet temperature T is raised by the Joule heat generated in this process. In this paper, we define the time taken for this large current discharge to end as t_{LCD}. Moreover, we assumed that the thermal runaway takes place in the cell, if the cell temperature exceeds the critical temperature until $t = t_{LCD}$, which can be estimated as 180 °C, since we can consider that the exothermal

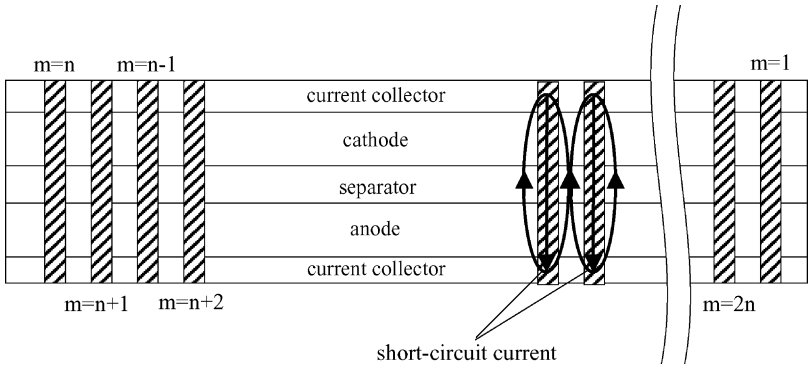

Fig. 7. Short-circuit model. When a nail penetrates a battery, the internal short-circuit occurs in the shaded regions successively in order of $m (1 \leq m \leq 2n)$ and the large current due to the short circuit is produced around the regions respectively. In our model, regarding the contact resistance between the current collectors as the resistance of the shaded regions, we simulated the distribution of the short-circuit current in the electrode sheet.

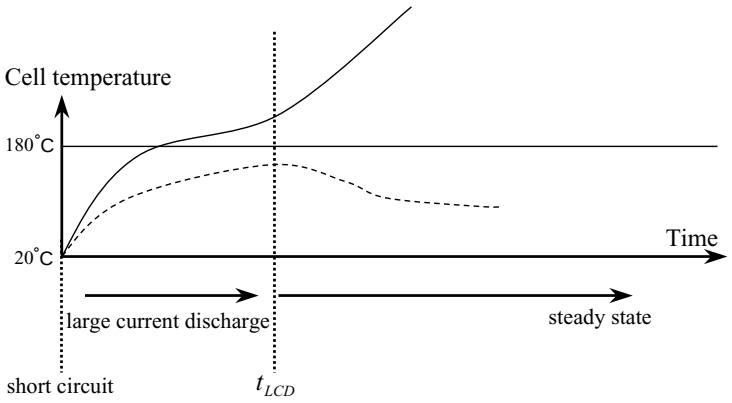

Fig. 8. Schematic diagram of the time variation of the cell temperature in the case of the internal short circuit. Solid line denotes the battery in which thermal runaway occurs in the nail penetration tests and broken line denotes the battery in which it does not occur.

reactions occur successively when the cell temperature is over 180 °C and the cell temperature increases rapidly within a few seconds [16]. Especially, around 180 °C, the chemical reaction at the anode/electrolyte interface and the thermal decomposition of the Li_xNiO_2 active cathode material have been reported to be most important [16,17]. In the case of the battery in which the thermal runaway takes place at the short circuit, the change in the cell temperature against time may be illustrated schematically as a solid line in Fig. 8. On the other hand, when the cell temperature does not attain 180 °C at t_{LCD}, we can consider that the lithium ion distribution in the cell approaches the equilibrium state slowly as it is limited by the diffusion in the cathode. Therefore, the increase of the cell temperature may be suppressed for the heat transfer between the battery and the environment, as shown in Fig. 8. According to the above discussions, we tackled the problem of the thermal runaway in the nail penetrating test.

The general energy balance for a lithium battery was studied theoretically in the papers [18–20]. In order to calculate $W(z, t)$ which corresponds to the amount of heat generated for a unit time in the unit volume of the electrode sheet in the case of the internal short circuit, we used the following equation derived in the paper [18].

$$W(z,t)\gamma_t = J_s(z,t)(V_p(z,t) - V_{p,rev}(z,t)) + J_s(z,t)T\frac{\partial V_{p,rev}}{\partial T} + \frac{\partial q}{\partial t} \quad (10)$$

where $V_{p,rev}$ stands for the cell voltage when the cell operates reversibly. Namely, the first term in Eq. (10) denotes the Joule heat due to the ohmic losses, including the energy dissipated in electrode overpotentials. Next, the second term is indicative of the entropic-heat and can be considered to be negligible in the discharge process of the cell using Li_xNiO_2 as an active cathode material and furthermore much smaller than the first term in general. We did not take into account the last term in the calculation of the total heat amount generated in the short-circuit process when $t \leq t_{LCD}$, since we assumed that the chain chemical reaction does not occur if the cell temperature does not exceed the critical temperature for thermal runaway. Therefore, we calculated only the first term. Here, $W(z, t)$ is averaged with respect to y by dividing the right-hand side of Eq. (10) by the total thickness of the cathode/separator/anode assembly γ_t. However, since most of the voltage drop represented by the first term in Eq. (10) occurs in the cathode, we can consider that the cell temperature increases in the cathode rapidly. Therefore, in practice, we took the thickness of the cathode γ_c for γ_t.

Moreover, we neglected the heat transfer in the cell and to the surroundings, since the rapid increase of cell temperature and the thermal runaway takes place within a few seconds after a nail is inserted in the battery. Therefore, we determined the increase in the cell temperature by dividing the total amount of the Joule heat generated during an interval t by the heat capacity of the electrode sheet.

$$\Delta T(z,t) = \frac{1}{H}\int_0^t dt' W(z,t') \quad (11)$$

where H is the specific heat of the electrode sheet, which has been found to be 2 J/(K cm^3) in the experiment [5,21]. We defined the cell temperature $T(z, t)$ as $T_0 + \Delta T(z, t)$, where T_0 is the room temperature (=293 K).

3. Results and discussions

We show the calculation results for the increase in the cell temperature in the nail penetration tests for batteries A and B. As shown in Fig. 7, we assumed that the internal short circuit occurs in the shaded regions successively in order of m ($1 \leq m \leq 2n$) during the time taken for a nail to penetrate the battery $\tilde{t}$, which was assumed to be 200 ms in this simulation. For simplicity, we regarded every distance between the short-circuit regions $\tilde{d}$ as 2.25 cm. Moreover, in regard to the actual battery, we can consider that the current collectors of the cathode and the anode are brought into contact with each other by the nail penetrating the battery and thereby the internal short circuit occurs. Thus, we measured the contact resistance between the current collectors and estimated its

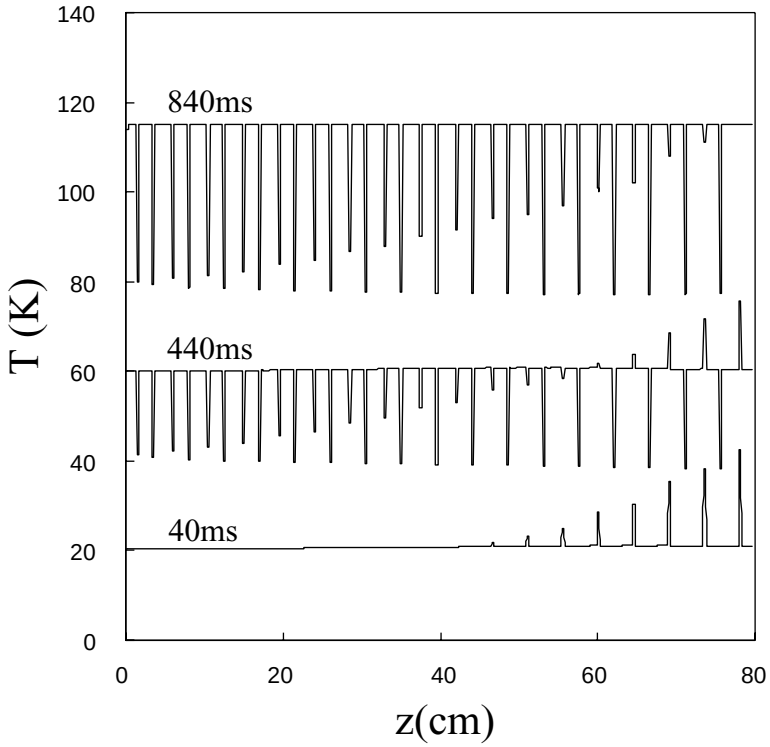

Fig. 9. Temperature distributions in the direction of z at the times 40 ms, 440 ms and 840 ms after a nail is inserted in battery B.

value as 0.6 Ω in our experiment. Regarding the resistance of the shaded region as 0.6 Ω, we simulated the distribution of the short-circuit current in the electrode sheet.

First, we show the temperature distribution in the direction z at the times 40 ms, 440 ms and 840 ms after a nail is inserted in battery B, respectively. As found in Fig. 9, since only a few short-circuit regions contribute to the discharge in the whole electrode sheet immediately after a nail is inserted in the battery, namely when $t \ll \tilde{t}$, the short-circuit current is concentrated in these regions and the temperature around these regions increases rapidly. However, once the nail penetrates the battery, the short-circuit current is distributed to the $2n$ short-circuit regions. Therefore, the temperature distribution in the regions, which the nail does not pass through, also becomes uniform. Noting that the thermal runaway is likely to take place even if the temperature at one point of the whole electrode sheet exceeds the critical temperature for it, we should compare $T_m(t_{LCD})$, which is defined as $\max\{T(z, t_{LCD})|0 \le z \le L\}$, with the critical temperature for it. Moreover, in our short-circuit model, we assumed that the cell temperature T_m has a maximum value when $t = t_{LCD}$, as discussed in Fig. 8. Thus, we plotted the calculation results of the time variation of T_m in the range below t_{LCD} for battery A as a solid line and for battery B as a broken line in Fig. 10, respectively. As shown in Fig. 10, the cell temperature for battery B exceeds the critical temperature for thermal runaway within 1.3 s, whereas, that for battery A does not even when $t = t_{LCD}$. Namely, this means that battery B with a better high-rate performance has a higher possibility for the thermal runaway to take place than battery A, although the battery B has a lower energy density. We can interpret these calculation results as follows. Since battery B has a lower internal resistance than battery A as

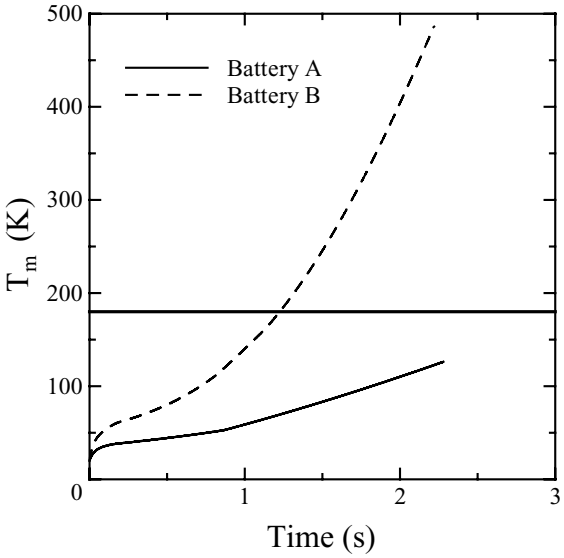

Fig. 10. Time variation of T_m in the case of the nail penetration test for batteries A and B. The calculation results of $T_m(t)$ are plotted in the time range below t_{LCD}. The horizontal thick line stands for the critical temperature for thermal runaway (=180 °C).

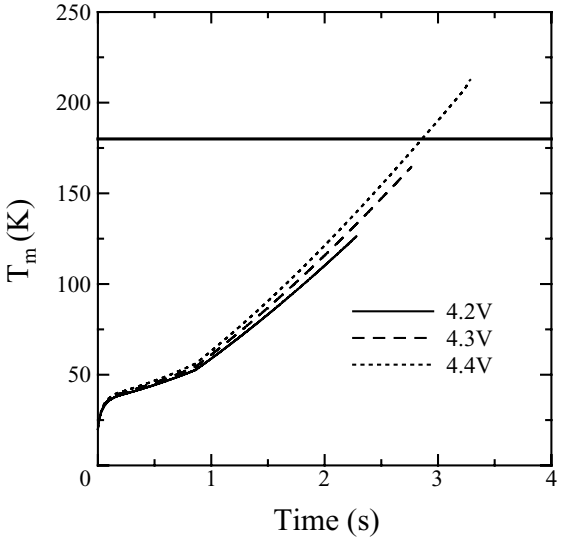

Fig. 11. Time variations of T_m in the cases of the nail penetration test for battery A charged with the three voltages 4.2 V, 4.3 V and 4.4 V. The solid line shows the same calculation result as that in Fig. 11. The horizontal thick line stands for the critical temperature for thermal runaway (=180 °C).

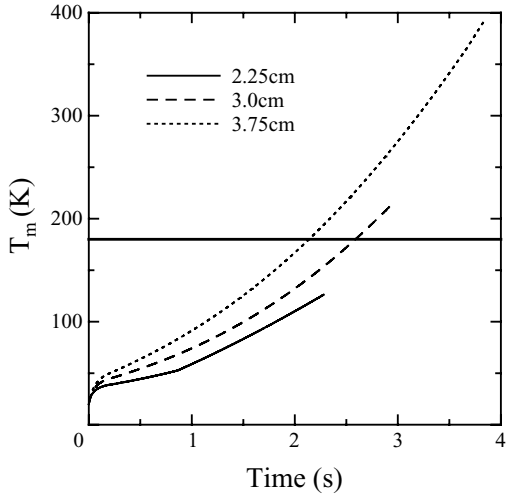

Fig. 12. Time variations of T_m in the cases of the nail penetration test for battery A, in the simulation of which the distance between the short-circuit regions $\tilde{d}$ is assumed to be 2.25 cm, 3.0 cm and 3.75 cm. The solid line shows the same calculation result as that in Fig. 11. The horizontal thick line stands for the critical temperature for thermal runaway (=180 °C).

shown in Fig. 1, the larger short-circuit current is produced in the electrode sheet of battery B. However, as found in Fig. 10, battery B has a value of t_{LCD} nearly equal to that of battery A, since the diffusion of lithium ion is much faster in the cathode of battery B. Therefore, we can consider that the larger amount of the Joule heat is generated in the nail penetration test in battery B than in battery A. Thus, we could provide a qualitative explanation of the experimental results [1]. Moreover, as found in Fig. 11, if we charge battery A with a higher voltage, the cell temperature shows a tendency to become larger in the case of the internal short circuit, because it takes longer to discharge the battery with a higher capacity. We can suggest that the thermal runaway is likely to take place in battery A in the nail penetration tests if its charge voltage is 4.4 V.

Next, we calculated the variation of the increase in the cell temperature in the nail penetration tests with the distance between the short-circuit regions $\tilde{d}$. We showed the calculation results in Fig. 12. This figure indicates that the possibility of thermal runaway in the battery increases as $\tilde{d}$ is larger. It can account for these calculation results that the section of the electrode sheet becomes wider for a larger value of $\tilde{d}$, which a short-circuit region plays a role of discharging. In addition, although we did not show the calculation results, we can also easily understand that the increase in the cell temperature in the nail penetration tests becomes larger for the same reason if it takes a larger $\tilde{t}$ to penetrate the battery. Thus, a theoretical explanation can be given to the following results observed often in the experiment. Namely, the possibility of thermal runaway in the battery is greater if we stop the nail just at the time when it passes through a few layers in the cell instead of penetrating the battery.

4. Conclusions

In this paper, we proposed a model of lithium secondary batteries which enables us to analyze both the charging/discharging characteristics and the increase of cell temperature in the case of the internal short circuit by giving the parameters corresponding to the proper fabricated electrodes. We showed the calculation results of the nail penetration tests for the batteries with different high-rate performances and discharge capacities, on the assumption that the Joule heat produced by the short-circuit current triggers the chain chemical reactions in the cell and leads to the thermal runaway if its total amount generated until $t = t_{LCD}$ exceeds the critical value. Especially, we focused on the results observed in the experiment [1] that a battery with a better high-rate performance has a higher possibility for the thermal runaway to take place in the nail penetration tests although its capacity is lower. It was found from the calculation results that both the magnitude of the short-circuit current and the time of discharge due to it (t_{LCD}) can account for the experimental results. Therefore, we can conclude that the lithium battery needs to be designed such that the rate performance satisfies the requirement that the capacity decreases rapidly for the current above $10C$ which corresponds to the short-circuit current, although it holds in the range of discharge current below $3C$. In addition, we may need to select the active materials whose chemical diffusion constant has dependence on temperature or lithium composition appropriate for achieving the required rate performance.

In this paper, although we did not discuss other tests on safety, such as the external short circuit test and crush test, our formalism may also be useful for the study of the increase in the cell temperature in those tests.

Acknowledgements

One of the authors (T.Y.) would like to thank Dr. H. Hasebe of Display Devices and Components Control Center, Toshiba Corporation for fruitful discussion.

References

[1] K. Kubo, I. Mitsuishi, S. Yamada, M. Kanda, in: Proccedings of the 42nd Battery Symposium in Japan, vol. 112, 2001, private communication.
[2] Y. Chan, W. Evans, J. Electrochem. Soc. 140 (7) (1993) 1833.
[3] C.R. Pals, J. Newman, J. Electrochem. Soc. 142 (10) (1995) 3274.
[4] C.R. Pals, J. Newman, J. Electrochem. Soc. 142 (10) (1995) 3282.
[5] K. Kanari, K. Takano, Y. Saito, Bull. Electrochem. Lab. 60 (12) (1996) 65.
[6] K. West, T. Jacobsen, S. Altung, J. Electrochem. Soc. 129 (7) (1982) 1480.
[7] S. Altung, K. West, T. Jacobsen, J. Electrochem. Soc. 126 (8) (1979) 1311.
[8] K. Mizushima, P.C. Jones, P.J. Wiseman, J.B. Goodenough, Mater. Res. Bull. 15 (1980) 783.
[9] K. Mizushima, KOTAIBUTSURI 15 (9) (1980) 619 (in Japanese).
[10] J. Fan, P.S. Fedkiw, J. Power Sources 72 (1998) 165.
[11] M.S. Ding, K. Xu, S.S. Zhang, K. Amine, G.L. Henriksen, T.R. Jow, J. Electrochem. Soc. 148 (10) (2001) A1196.
[12] R.A.M. Hikmet, M.P.J. Peeters, J. Lub, W. Nijssen, J. Electrochem. Soc. 146 (7) (1999) 2397.
[13] J. Newman, Electrochemical Systems, Prentice Hall, Englewood Cliffs, NJ, 1991.
[14] P.G. Bruce, A. Lisowska-Oleksiak, M.Y. Saidi, C.A. Vincent, Solid State Ionics 57 (1992) 353.
[15] N. Takami, A. Satoh, M. Hara, T. Ohsaki, J. Electrochem. Soc. 142 (2) (1995) 371.
[16] S. Tobishima, J. Yamaki, J. Power Sources 81–82 (1999) 882.
[17] Y. Isozaki, I. Mitsuishi, Y. Satoh, M. Kanda, in: Proceedings of the 41st Battery Symposium in Japan, vol. 390, 2000.
[18] D. Bernardi, E. Pawlikowski, J. Newman, J. Electrochem. Soc. 132 (1) (1985) 5.
[19] H.F. Gibbard, J. Electrochem. Soc. 125 (3) (1978) 353.
[20] L. Rao, J. Newman, J. Electrochem. Soc. 144 (8) (1997) 2697.
[21] K. Kanari, Y. Saito, Netsu Bussei 10 (1996) 59 (in Japanese).